Notch tolerance of high-strength Cu-based nanocomposites

Rongmei Niu and Ke Han*
National High Magnetic Field Laboratory/Florida State University
1800 E Paul Dirac Dr. Tallahassee, FL 32310, USA
E-mail: han@magnet.fsu.edu

Abstract:

Understanding flaw tolerance in composites is critical for both the design and the application of reliable structural materials. Through uniaxial tension experiments, we explored notch-related plastic deformation mechanisms in both Cu-alumina and Cu-Ag-Zr composites via real-time strain mapping. Experiments demonstrated that, in samples under tensile loading with notch pairs from both materials, highly strained regions first emerged from notch tips and then developed into strain-concentration bands. Under further loading, each of these bands changed in shape from straight to elliptical as it formed a bridge across to its opposite notch tip. When any sample came under tension, its notch tip radius increased, and its strain-concentration bands gradually moved toward its notch segment center. High plastic strain became localized at the notch tips, of course, but also within the strain-concentration bands. Notch-strengthening, on the other hand, appeared mainly within the strain-concentration bands. The two composites showed different ductility within these bands. Alumina-particle-strengthened Cu had low elongation that eventually resulted in an abrupt fracture somewhere within these bands. By contrast, Ag-fiber-strengthened Cu-Ag-Zr composites had high elongation in strain-concentration bands, accompanied by clear notch blunting. In other words, Ag-fiber-strengthened Cu had higher flaw tolerance than alumina-particle-strengthened Cu, a difference we attributed to the differences between malleable fibers and hard particles.

Keywords: Flaw tolerance, notch geometry, notch strength, strain-concentration bands, fracture

1. Introduction

Cu-based composites are used in numerous applications that require optimized combinations of mechanical strength with either electrical or thermal conductivity. The strength of Cu composites is enhanced through dislocations [1-3], grain refinement [4, 5], and dispersion

strengthening [6-11]. Typical conductor materials for high-field magnets are Cu-based, fiber-reinforced nanocomposites (such as Cu-Ag [12-22] and Cu-Nb [1, 2, 23-30]) and particle-reinforced composites (such as Cu-alumina [6, 7, 31-33] and Cu-Cr-Zr [34-38]). For desired mechanical strength, each of these conductor materials must have a nanostructure, i.e. a microstructure that reaches nanoscale.

The fabrication of nanostructured, high-strength conductors requires severe plastic deformation, which may cause such structural defects as voids, internal cracks, or second-phase particles. Surface damage (deep scratches, gouges, grooves, or dents) is also inevitable[39]. The presence of such defects is known to increase stress concentration. Researchers use the term "notch sensitivity" to describe the reduced ductility that occurs when a triaxial stress field is combined with steep stress gradients like those that often occur near any defect, like a notch [40]. In ductile materials, plastic flow may reduce stress concentration near a notch tip. In brittle materials, however, no such relief mechanisms exist--stress concentration is maintained right up to the point of fracture.

In fine-grained nanocomposites, however, notch sensitivity may be expected to be different from that of their coarse-grained counterparts [41-43]. In nanomaterial design, the widely used engineering concept of "stress concentration at flaws" does not apply because certain materials, like nanocrystalline metal, become insensitive to flaws at nanoscale [44]. Kumar et al. proposed that apparent notch insensitivity at nanoscale arises from the breakdown of classical fracture mechanics in thin films [45]. Nano-grain realignment or rotation in the absence of dislocations causes extreme stress homogenization at notch tips and makes stress concentration irrelevant at nanoscale. In a material where microstructure is dominated by grain boundaries, realignment or rotation of crystals commonly occurs, but it is currently unknown whether such phenomena can take place in nanocomposites, in which interfaces dominate.

Inspired by differences in sensitivity to notches, we focused in this work on notch-tip stress concentrations by comparing a fiber-strengthened, nanostructured composite to a particle-strengthened, microstructured material. For microstructured material, we investigated Cu-alumina, a composite strengthened by non-deformable, ceramic nanoparticles. For a nanostructured composite, we chose Cu-Ag-Zr, a composite strengthened by malleable, metallic fibers [46-48]. Although two composites have different strengthening mechanisms, they are conductors for high-field magnets. Cu-alumina and Cu-Ag-(Zr) have different combination of

mechanical strength and electrical conductivity. High electrical conductivity (~82%IACS, International Annealed Copper Standard) is the advantage of Cu-alumina, despite its moderate strength (~560MPa)[7]; High strength (>800MPa) is often reflected in Cu-Ag-(Zr), despite its moderate electrical conductivity(~75%)[18, 20, 22, 24, 25, 49, 50]. The unique properties made them have different applications. So far, no published research has directly addressed the influence of notches on the strength and plasticity of Cu-alumina and Cu-Ag-Zr together. The purpose of the current work is to provide insight into the effect of notches on mechanical properties in Cu-based composites with different microstructures.

2. Experimental methods

In this investigation, we used rectangular wires of Cu-1.1wt%Al_2O_3, 5.2 x 8.6 mm^2, drawn by Sam Dong, and Cu-7wt%Ag-0.05%Zr, 4 x 6 mm^2, supplied by Leibniz-Institut für Festkörper- und Werkstoff-Forschung (IFW), Dresden.

All unnotched tensile samples were machined from wire samples and had a dog-bone profile. For Cu-1.1wt% alumina, the gauge length was 4.0 mm and the gauge width was 4.3 mm (see Fig.1). For Cu-Ag-Zr, the gauge length was 4.0 mm and the gauge width was 3.0 mm.

To examine the mechanics of constrained yielding, pairs of V-shaped notches were cut perpendicular to the loading axis on either side of the plank-like section crossing from one side of the notch to the other. The notches were machined within the 4.0 mm gauge length. The cross-section area of a sample between notch pair tips was one-half the remaining area of the sample lying outside the notches but within the gauge length. The notch angle was held constant at 60 degrees. The Notch Tip Radius (NTR) ranged from 0.20 mm to 3.83 mm, as measured using the video system iNEXIV VMA-2520.

Tensile tests were carried out on both notched and unnotched samples on a servo-hydraulic MTS test machine with a load cell of 20KN. All samples were measured using x-y-z coordinates, with x indicating the longitudinal direction of drawing or rolling, y indicating the transverse direction (width), and z indicating the short-transverse direction (thickness). The tension axis was parallel to the x-axis. The specimens were carefully aligned along the loading axis and subjected to increasing tension until fracture occurred. Notch strength (σ_N) was defined as the maximum load divided by the net cross-sectional area at the notch. The error of measured strength values was below xx.

A Digital Image Correlation (DIC) system was employed to monitor real-time strain in the vicinity of notch tips. To understand local plastic deformation properties, we measured the average strain in an area of 0.1x 0.1 mm^2 within strain-concentration bands (see Fig. 1e). The elongation reported in this work refers to the strain needed to initiate cracks, but not to cause fracture. Since the strain in this study was measured locally by DIC at the notch tips and was not averaged to undeformed areas, it better reflects the real plasticity in the deformed area.

Microstructure and fracture morphology were examined by dual-beam scanning electron microscopy (FEI Helios G4 UC). Low magnification fracture images were observed by light microscopy (Nikon iNEXIV VMA-2520).

3. Results and discussion

3.1 Notch tip strain evolution in Cu-alumina

In each Cu-alumina wire sample without notches, a necking region appeared within the gauge length under tension. The highest strain occurred in the center of this necking region, where we measured local strain as high as 34%, nearly 3 times the overall average strain (13%) within the total 4 mm-gauge length (see Fig.1b, the red region).

With the introduction of double-edged notches, not only was the maximum local strain reduced, but the highly strained necking region was also redistributed. The necking region was separated into two strain-concentration bands. The area of highest strain shifted from the necking center to the notch tips.

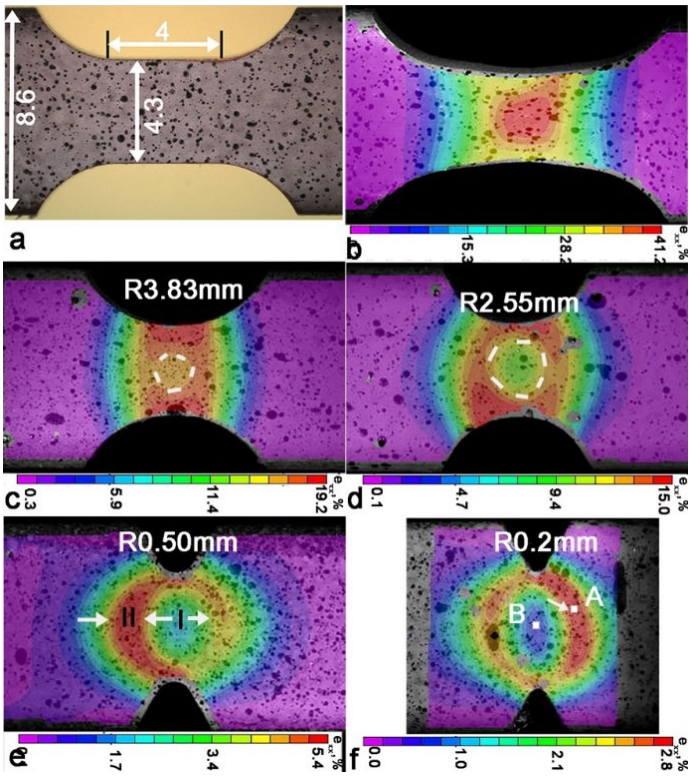

Fig. 1 Real-time observation of necking in Cu-alumina wires. The color bars index the tensile strain levels in the samples. (a) Geometry of dog-bone samples. Gauge length=4.0 mm; cross-section width=4.3 mm (half of the original width); thickness=5.2 mm. (b) Necking distribution after yielding in dog-bone samples. (c-f) Strain-concentration in double-edged notch samples. White dashed lines mark a boundary between the high strain and the ultra-high strain areas. In (c) NTR = 3.83 mm, in (d) NTR = 2.55 mm, in (e) NTR = 0.50 mm, and in (f) NTR = 0.20 mm.

Necking locations changed with the introduction of a notch pair into the edges of each sample. In a sample with NTR of 3.83 mm, necking was concentrated in the narrowest section between the pair of notches. Close observation of this sample, however, revealed an island of lower strain (15%) in the very center of the narrowest section (see Fig. 1c, the white circle). In the regions surrounding that island, strain was about 4% higher (~19%), especially in the notch tip areas (Fig.1c). In a sample with NTR of 2.55 mm, the inner island was bigger, separating the strain-concentration region into two parts. The strain difference in that sample between the strain-concentration region (15%) and the island (9%) was greater than in the sample with an NTR of 3.83 mm (see Fig.1d). In samples with an even smaller NTR, the two strain-concentration bands were more widely separated, creating an elliptical loop around the inner island. Using this loop as a baseline, we defined two deformation zones: Zone I, the inner island,

was defined as the segment between notches; Zone II, containing the most deformed areas (otherwise known as the strain-concentration bands) was characterized by a dense strain-gradient distribution. We deduced from the strain difference between Zone I and Zone II that sharper notches would significantly reduce the magnitude of strain exerted on the notch segment center.

Table 1 Notch-size-dependent mechanical properties in Cu-alumina wires

Notch tip Radius, mm	σ_N or UTS*, MPa	NSR	Elongation in necking, % Site A	Elongation in center, % Site B
0.20	682	1.19	3.6±0.6	0.8±0.4
0.50	672	1.17	4.5±1.2	1.9±0.5
1.28	653	1.14	6.6±3.0	2.5±0.8
1.94	649	1.13	7.3±3.3	5.3±1.7
2.55	640	1.12	11.6±4.2	9.1±2.8
3.83	622	1.08	16.7±3.5	13.6±3.2
+∞	573	1.00	34±7.2	34±7.2

* σ_N represents notch strength for notched samples and UTS for unnotched samples.

* Notch tip radius was measured values.

* Elongation was measured from a rectangular area of 0.1 mm x 0.1 mm at the notch tip (NT).

To quantify the strain difference in each zone, we analyzed two representative sites: Site A was at the center of Zone II, away from the notch, and Site B was at the segment center between the pair of notches. Each of these sites measured 0.1 x 0.1 mm^2. The NTR-dependent elongation values at both sites are summarized in Table 1. Site A experienced more plastic deformation than Site B, but at both sites, elongation decreased as NTR decreased. For a sample with NTR of 3.83 mm, elongation decreased by 51% (from 34±7.2% in a sample without notches to 16.7±3.5% at Site A in a sample with notches); at Site B, elongation decreased to 13.6±2.6 %. For samples with NTR of 0.50 mm and 0.20 mm, the elongation value at Site A decreased to 4.5±1.2 and 3.6±0.6%, respectively. At Site B, elongation decreased to 1.9±0.5% and 0.8±0.4%, respectively.

Next, the size of notches changed the stress-strain behavior at notch tips, especially for sharp notches. In the nominal elastic stage of Zone I, the slopes on the stress-strain curves were in a range of 108~115 GPa for NTRs above 0.5 mm, which is the typical Young's modulus of

Cu-alumina[7]. It increased to 144 GPa at NTR of 0.50 mm and 170 GPa at NTR of 0.20 mm (Cf. Fig.2a).

A notch in a sample not only affected the elongation of that sample, but also its Ultimate Tensile Strength (UTS). In Cu-alumina wires, we observed a notch-strengthening effect. The UTS of unnotched Cu-alumina wires was 573MPa, which was close to the previous reported value of 565 MPa [9]. Notch strength (σ_N) reached its maximum of 682 MPa at NTR 0.20 mm, an increase of 19% over the UTS of unnotched samples (see Table 1).

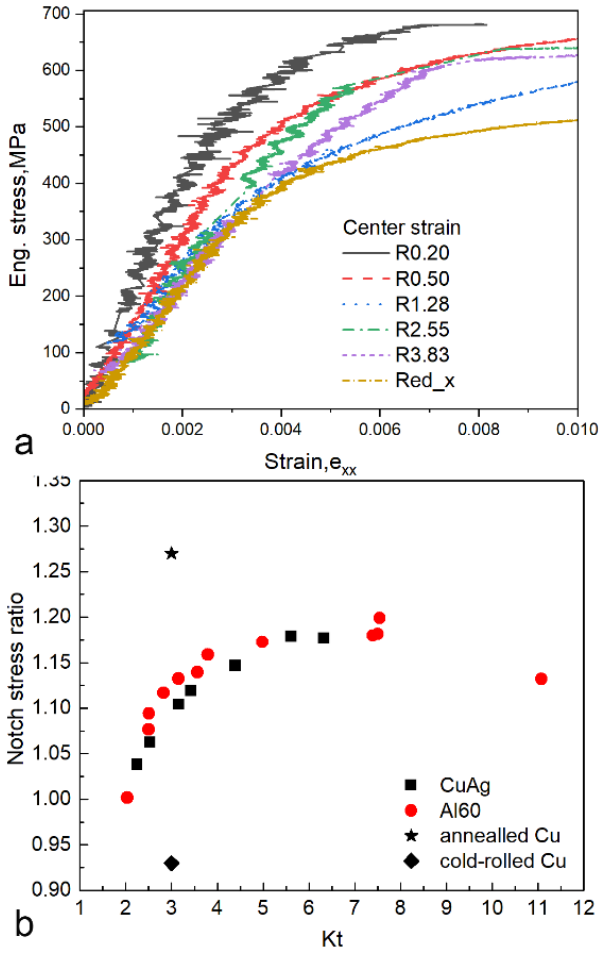

Fig. 2 (a) Stress-strain curves in the nominal elastic stage of Zone I. (b) NSR as a function of Kt in Cu-Ag-Zr and Cu-alumina. Annealed Cu and rolled data were taken from Ref[51].

Notch Strength Ratio (NSR), as calculated by σ_N/UTS, depends on notch geometry, which can be described by the stress concentration factor K_t [40, 51]. We calculated K_t as follows: $K_t = 1 + 2 \times \sqrt{h/R}$, where h is the distance between notch tips and R is the notch radius [52]. NSR values ranged from 1.08 to 1.19 in Cu-alumina (see Table 1). With the same

notch radius, NSR values of Cu-Ag-Zr ranged from 1.04 to 1.18 [53]. This range is slightly lower than in Cu-alumina (see Fig. 2b). A lower NSR number indicates lower strengthening capacity. The UTS of Cu-Ag-Zr without notch was about 990 MPa, which was lower than that of Cu-5Ag-0.1Zr, Cu-7Ag[20, 21], but higher than that of Cu-3Ag-0.05Zr[21] and Cu-24Ag[49]. The notch-strengthening effect of Cu-Ag-Zr and Cu-alumina was either lower than that of annealed pure Cu (NSR=1.27 at Kt of 3) or higher than that of cold-rolled pure Cu (NSR=0.93 at Kt of 3) [51].

3.2 Strain mapping in Cu-Ag-Zr wire

In our Cu-1.1wt%Al_2O_3 wires, which had been strengthened by nano alumina particles, strength reached only about 600 MPa, but in our Cu-Ag-Zr wires that had been strengthened by nanoscale Ag fiber, strength reached 990 MPa. Because of different strengthening mechanisms and different UTS levels, these two composites showed different deformation behavior in regions near notches.

The typical plasticity of high-strength Cu-Ag is not more than 8% in elongation [20, 49, 54]. According to the constant volume law, the Reduction-in-Area (RA) at fracture should be around 7%. The RA in high-strength CuAg wire, however, is usually much higher, ~48~64% [49]. This suggests that deformation in Cu-Ag wire is highly localized upon fracture. Taking account of this, we investigated tensile samples with a short gauge length of 4 mm (see Fig .3a). Within the gauge length in samples without notches, a necking area gradually formed upon tension deformation. In this necking area, we found that cracks started to form after local elongation reached 50% (see Figs. 3b and 3d). This value was significantly higher than that of Cu-alumina (34%). Beyond this point, the speckles that we had printed onto our sample had become so deformed that our DIC software could no longer produce accurate strain analysis (see Fig.3c). Therefore, based on the correlation trend between the average strain and the strain in the local necking area, we extrapolated fracture strain of about 90% at the necking center (see Fig.3d).

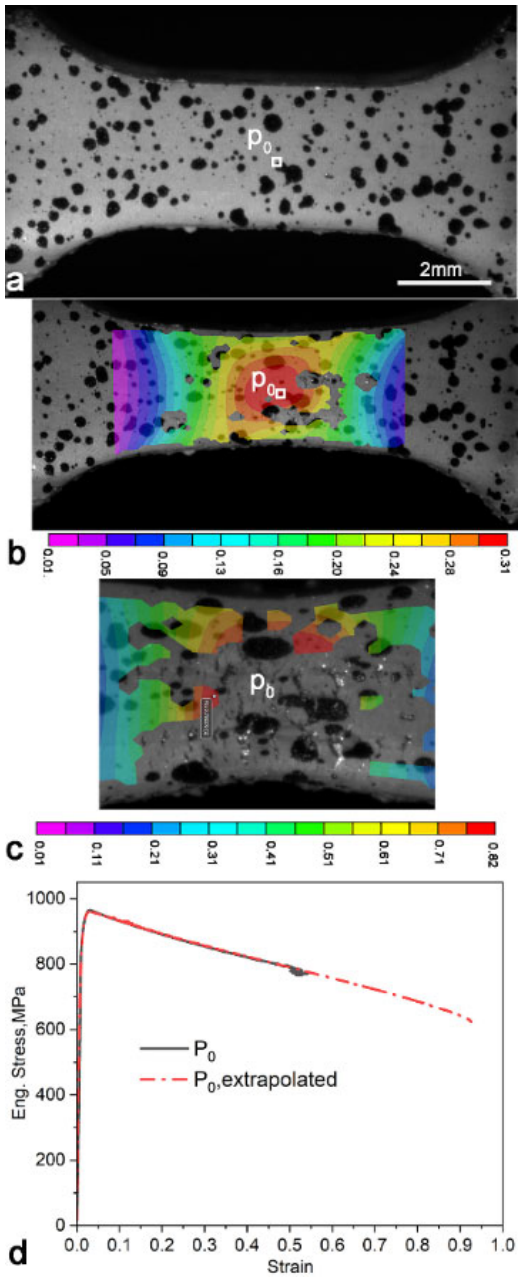

Fig. 3. Strain values obtained by DIC in a Cu-Ag wire. (a) Original image of a reduced cross-section sample with a width of 3 mm and a gauge length of 4 mm. The black dots (speckles) are painted markers for strain measurement using DIC; (b) Nonuniform strain distribution along the gauge length, showing that a highly strained area starts to localize in the red region. The color bar indicates the tension strain level; (c) Pronounced necking at the center of the gauge length. In this location, the grey area indicates where speckles are so severely stretched under tension that DIC can provide no strain data; (d) Extrapolated tensile strain in the necking area. The elongation at P_0, indicated by the white square, is

50%, measured from DIC result. The fracture strain at P_0 can reach as high as 90%, based on the correlation trend between average strain and local strain.

The presence of double-edge notches in Cu-Ag-Zr wire (as in the Cu-1.1wt%Al_2O_3 wires discussed in section 3.1) changed not only the location of necking, but also the strain magnitude within the strain-concentration area. In samples with large NTRs (3.83 mm or 2.55 mm), strain-concentration bands were concentrated in the segment center. Strain values differed very little between Zones I and II (Cf. Figs. 4 a-l). The values of elongation in the sample with NTR of 3.83 mm were 48% in Zone I and 55% in Zone II, a difference of only 7%. In the sample with NTR of 2.55 mm, elongation values were only 37% in Zone I and 45% in Zone II. In samples with small NTRs (1.02 mm or 0.50 mm), strain-concentration bands reached outward beyond the notch segment into the unnotched region, and the area of Zone I was larger in these samples than in samples with larger NTRs. Elongation values were smaller in samples with smaller NTRs than in those with larger NTRs. In the sample with NTR of 1.02 mm, for example, the elongation values were 20% in Zone I and 33% in Zone II, which were respectively about 46% and 27% smaller than in samples with NTR of 2.55 mm. The elongations in the sample with NTR of 0.50mm dropped further to 7% in Zone I and 27% in Zone II (Cf. Figs. 5a and 5b). Accompanying the plastic deformation in Zone II, many cracks appeared within strain-concentration bands (Cf. Figs. 4b, 4e,4h, 4k).

Deformation was NTR-dependent, not only in the plastic deformation regions but also in the nominal elastic regions (Zone I). In the elastic stage, the slopes on the stress-strain curves were 122±8 GPa, 137±5 GPa, 175±2 GPa, and 196±2 GPa at NTRs of 3.83 mm, 2.55 mm, 1.02 mm, and 0.50 mm, respectively (Cf. Fig.5c). With an NTR of 3.83mm, the slope value was only 6% higher than the Young's modulus of Cu-Ag (115GPa) [49]. In the sample with sharp notch tips (0.50 mm), the slope values (196±2 GPa) were almost twice as high as the Young's modulus of Cu-Ag-Zr. Based on these slope values, we deduced that Zone I of samples with sharp notches was subjected to much less stress concentration than Zone II of the same samples.

The curvature of the strain-concentration bands was larger in samples with smaller NTRs. The inner radius of Zone II, as measured before failure, was as follows: 9.2± 0.9mm for NTR of 3.83mm, 4± 0.5mm for NTR of 2.55mm, 2.3± 0.2mm for NTR of 1.02mm, and 2.1± 0.1mm for NTR of 0.50mm. During deformation, the NTR of all samples increased, i.e. the tip became blunter. The extent of the bluntness depended on the initial NTR of the sample. In samples with

initial NTRs of 3.83±0.05 mm, 2.55±0.03 mm,1.02±0.03 mm, and 0.50±0.04 mm, the final NTR before failure increased to 4.81±0.76 mm, 3.98±0.17 mm, 1.86±0.07 mm, and 2.08±0.12 mm, respectively. Notch blunting was not obvious in Cu-alumina because of low elongation values in Zone II (Cf section 3.1).

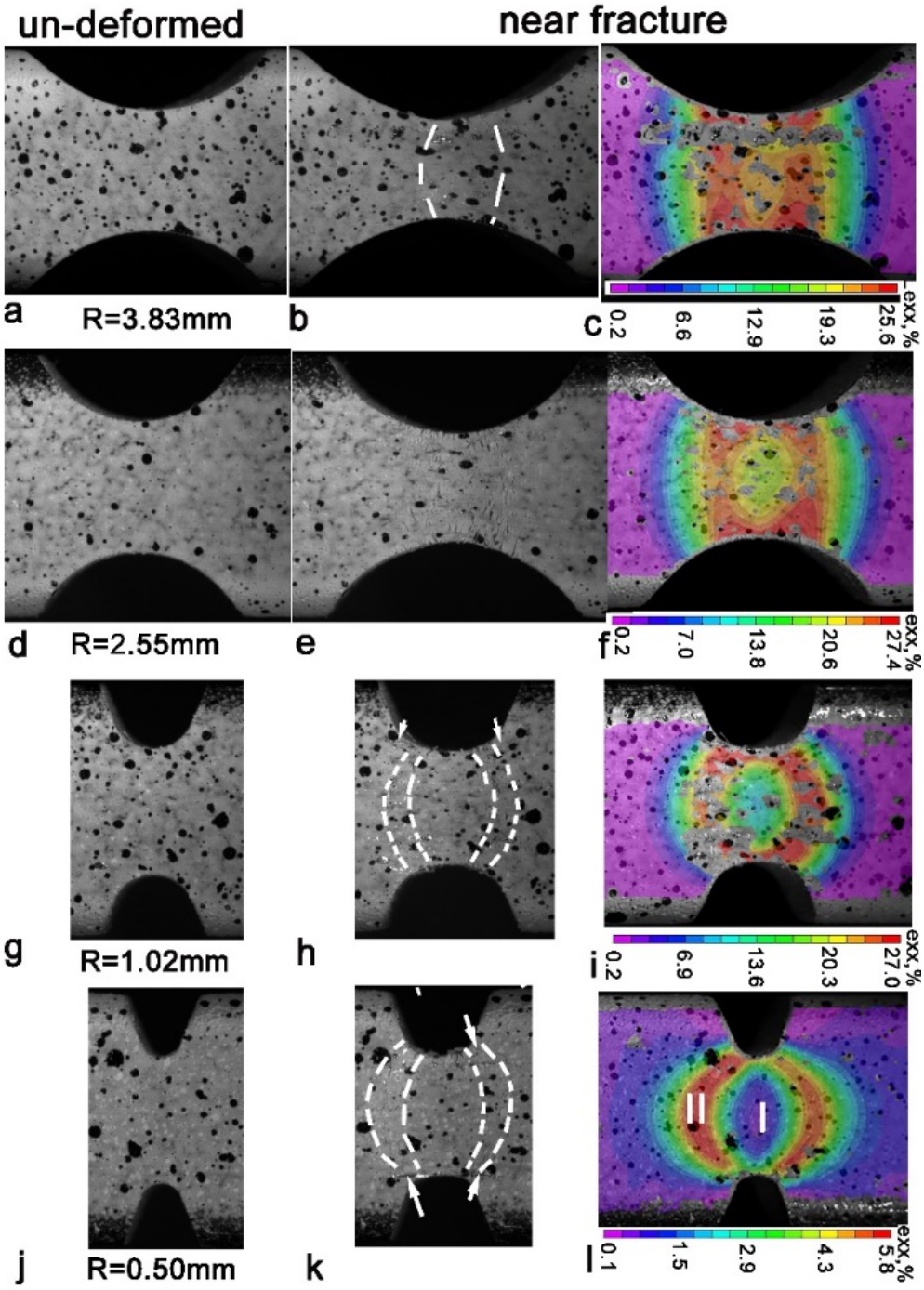

Fig. 4 Real-time observation of local plastic deformation and crack development in notched Cu-Ag-Zr samples. In (a), (d), (g), and (j), double-notched samples are shown before tension. The tension direction

is along the horizontal direction. In (b), (e), (h), and (k), microcracks appear at the notch tip right before fracture. The white dash lines outline cracks and fractured locations. In (c), (f), (i), and (l), images show DIC strain mapping related to samples in (b), (e), (h), and (k), respectively. In (a-c), NTR=3.83 mm; in (d-f), NTR=2.55 mm; in (g-i), NTR=1.02 mm, in (j-l), NTR=0.50 mm.

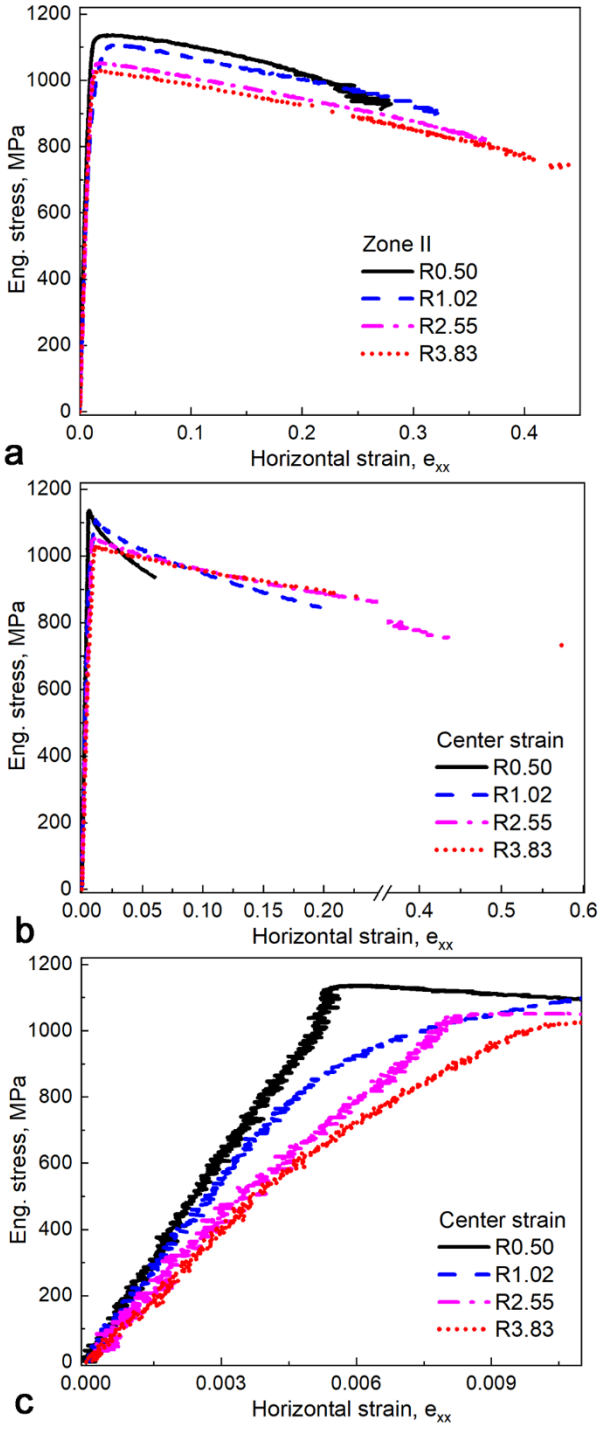

Fig. 5 NTR-dependent strain evolution in Cu-Ag-Zr. (a) e_{xx} at notch tips in Zone II; (b) Strain levels at the center of Zone I; (c) Center strain levels of Zone I at elastic stages.

3.4 Microstructure at necking

After tensile tests, we examined microstructures in the necking regions of unnotched samples using SEM. We observed no secondary cracks in the vicinity of the fracture surface in Cu-alumina wires (see Fig. 6a). Alumina ceramic particles appeared as either black or white dots against a grey background. The particles that appeared on the 6 mm-wide surfaces were distributed along the wire axis and varied in size from 5 nm to 4 μm. Pure Cu is highly ductile, with significant plastic deformation capacity. The extremely high hardness of alumina (Vickers hardness ~15–20 GPa) is rigid and brittle. Because of the hard and un-deformable nature of alumina, de-cohesion of the interface between the alumina particles and the matrix was inevitable, resulting in the formation of short micro-cracks between the particles and the matrix during cold-drawing fabrication (see Fig. 6b). Under tension, necking regions were subjected to ~34% elongation. Consequently, the short micro-cracks between the particles and the matrix propagated and coalesced both laterally and longitudinally (see Fig. 6c). The final fracture path was the result of the coalescence of these micro-cracks. Meanwhile, the copper grains in our sample were greatly elongated in the necking region (see Figs. 6a and 6b). The average grain size within the designated necking region was ~3.1 μm, 46% longer than the average grain size of ~2.4 μm found in regions outside of the designated gauge length.

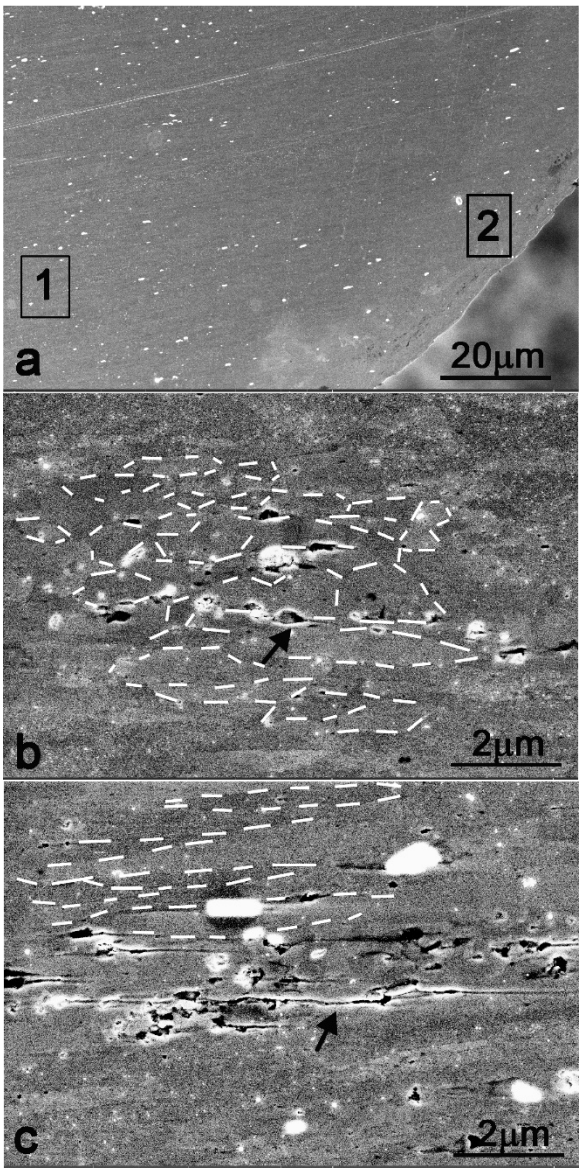

Fig.6. SEM images of alumina particle distribution and de-cohesion: (a) A low-magnification image in a necking region at the fractured area in an unnotched Cu-alumina sample. The white dots are alumina particles. Tensile axis is horizontal. (b) A high-magnification image taken in the rectangular region 1 in Fig. (a) that is outside of the gauge length. De-cohesions and short micro-cracks are seen around alumina particles. Dashed lines indicate the grain boundaries of the Cu-matrix; (c) A high-magnification image taken in the rectangular region 2 in Fig. (a), where necking occurs. Micro-cracks propagate and coalesce. Dashed lines indicate the grain boundaries of the Cu-matrix.

By contrast, unnotched Cu-Ag-Zr samples demonstrated different fracture behavior from that of unnotched Cu-alumina samples. The former showed not only longer elongation, but a

greater number of intersecting primary cracks in the fracture regions (see Fig. 7a). These cracks inclined about 44° in the tensile direction in Cu-Ag-Zr.

Upon deformation, the deformable Ag fibers, which formed larger interface areas with the matrix, behaved differently in Cu-Ag-Zr from the un-deformable alumina particles. The alignment of the alumina particles was not obvious, but all of the Ag fibers remained clearly aligned along the tensile axis (see Fig.7b). In the aligned region, several slip systems operated, each in its preferred orientation. The slip planes were roughly parallel to the primary cracks for fracture (see Fig.7c). A schematic was employed to illustrate the difference between Cu-alumina and Cu-Ag-Zr on their fracture mechanisms (see Fig. 8).

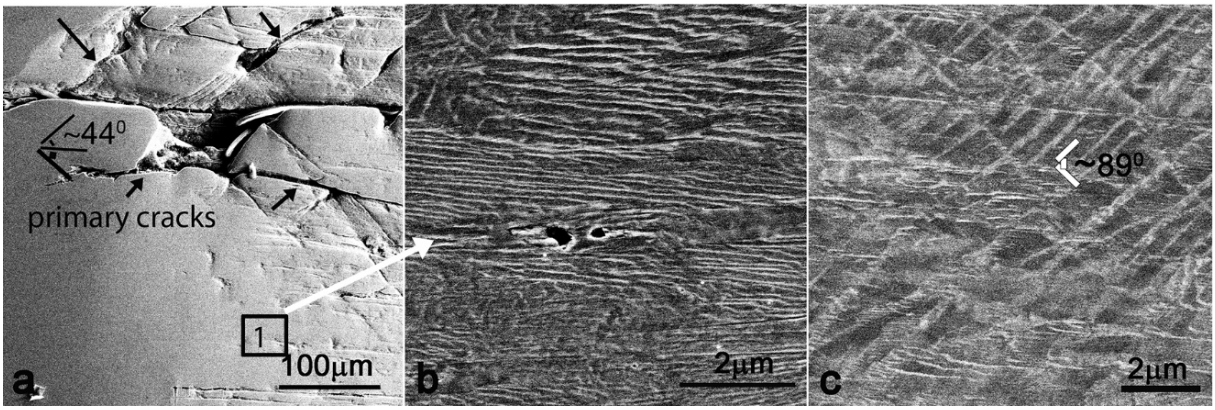

Fig. 7. Microstructure evolution with tension deformation in unnotched Cu-Ag-Zr wires at different locations. The tensile axis is parallel to the horizontal direction. (a) Fracture in the necking region. The angle of inclination of primary cracks, indicated by black arrows, is ~44±1° to the tensile axis; (b) A close-up view of the microstructure in the region identified as "1" in Fig. (a), which is located near the cracking area. Stretched Ag fibers (white contrast lines) align with tension direction; (c) Two operating slip systems along shear direction. Slip directions are roughly aligned with the primary cracks.

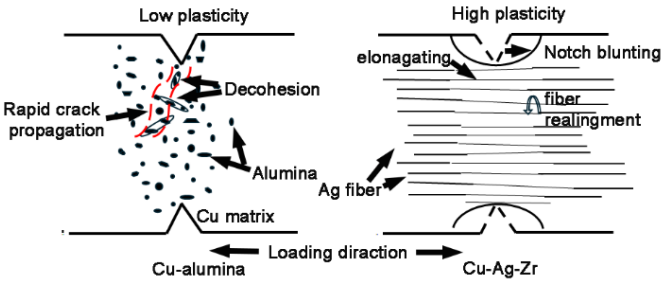

Fig. 8 A schematic illustrating the fracture mechanisms in Cu-Alumina and Cu-Ag-Zr. In Cu-alumina: No notch blunting, rapid decrease in local elongation, and crack propagation accelerated by decohesion,

indicating low flaw tolerance. In Cu-Ag-Zr: Pronounced notch blunting, slow decrease in local elongation, and fiber realignment contributing to larger interface areas and greater flaw tolerance.

3.4 Fracture morphology

In both notched Cu-alumina and notched Cu-Ag-Zr bulk wires, plastic deformation was localized in strain-concentration bands. The width of the deformed bands after failure was estimated using optical microscopy along the tension direction. In any given sample, the smaller the NTR, the narrower the strain-concentration bands. Because of the plasticity difference between Cu-alumina and Cu-Ag-Zr, strain-concentration bands were not continuous in Cu-alumina and were continuous in Cu-Ag-Zr (see Figs. 9 and 10). Because of the low elongation of Cu-alumina, the region was not clearly defined enough to allow for measuring the width of the strain-concentration bands there. In Cu-Ag-Zr, however, the region of strain-concentration bands was clearly defined. The average width of strain-concentration bands in Cu-Ag-Zr wires was 0.8±0.1mm at R0.20 mm, 0.9±0.1mm at R0.50 mm, 1.0±0.1mm at R1.02 mm, 1.3±0.1 mm at R1.28 mm, 1.7±0.2 mm at R2.55 mm, and 1.7±0.5 mm at R3.83 (see Fig.10). Obviously, the presence of notches not only undermined local plasticity but also limited the width of the strain-concentration bands.

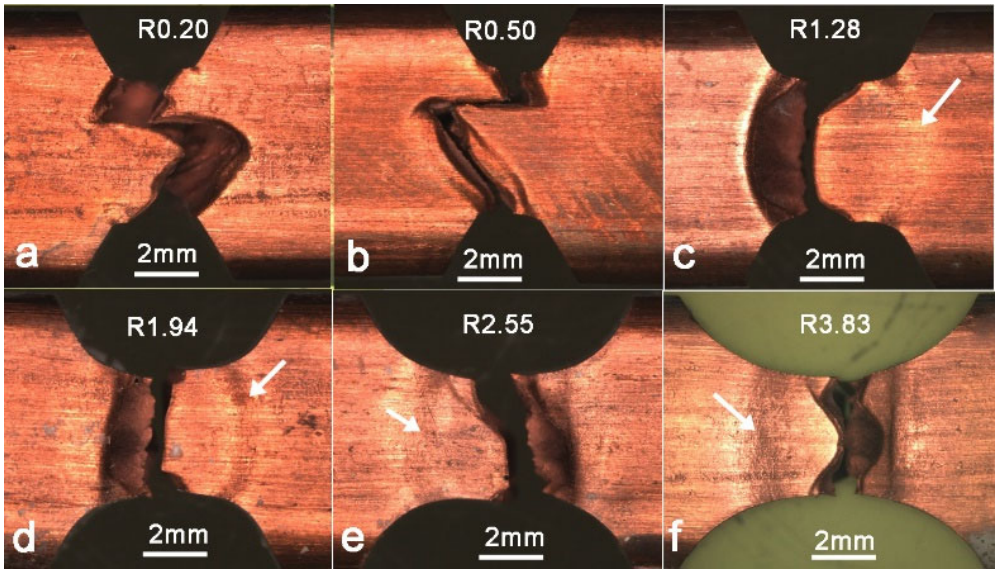

Fig. 9 Images of fractured samples of Cu-alumina wire at different notch radii under an optical microscope. a). R=0.20 mm; b). R=0.50 mm; c). R=1.28 mm; d). R=1.94 mm; e). R=2.55 mm; f). R=3.83 mm. The tension direction is parallel to the longitudinal direction. The white arrow indicates the strain-concentration bands.

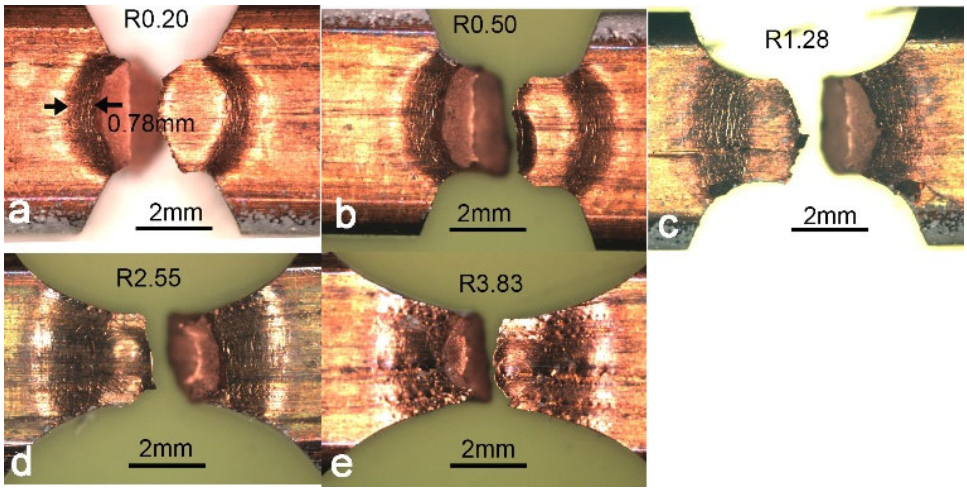

Fig. 10 Images of fractured samples of Cu-Ag-Zr wire at different notch radii under an optical microscope: a). R=0.20 mm; b). R=0.50 mm; c). R=1.28 mm; d). R=2.55 mm; e). R=3.83 mm.

The fracture surfaces of our samples, which contained different notch tip radii, were all roughly perpendicular to the applied load. A common feature observed on these fracture surfaces was the presence of shear lips (*Fig.* 11). Fibrous tearing caused by shear loading may be the failure mechanism in samples with small NTRs. In the center of the fracture surface in the sample with a small NTR (0.50 mm), we observed that the width of any two shear lips taken together was more than twice that of the dog-bone-shaped final fracture zone between the two lips (Fig. 11a). Within each shear lip, small parabolic-shaped dimples appeared (Fig. 11b). The fracture surfaces in the final fracture zone were characterized by a cluster of larger, oval dimples (see Fig.11c). We observed that further plastic deformation ceased once smaller oval dimples were formed, but the question remains whether the same is true of the larger dimples.

In samples with larger NTRs, different features emerged. Shear lips were narrower, for example. With an NTR of 3.83 mm, the final fracture zone dominated while the shear lips nearly disappeared (see Fig.11d). In addition, the fracture surface had become rougher than in samples with smaller NTRs. Near the edges of the fracture surface, the dimples now showed bimodal size distribution. The smallest dimples were less than 1 μm, and the largest were as big as 8 μm (Fig. 11e). Fracture surfaces were mainly composed of dimples that were large (5~30 μm) and spherical rather than small and parabolic. The failure mechanism in samples with larger NTRs was identified as microvoid coalescence rather than fibrous tearing (Fig. 11f).

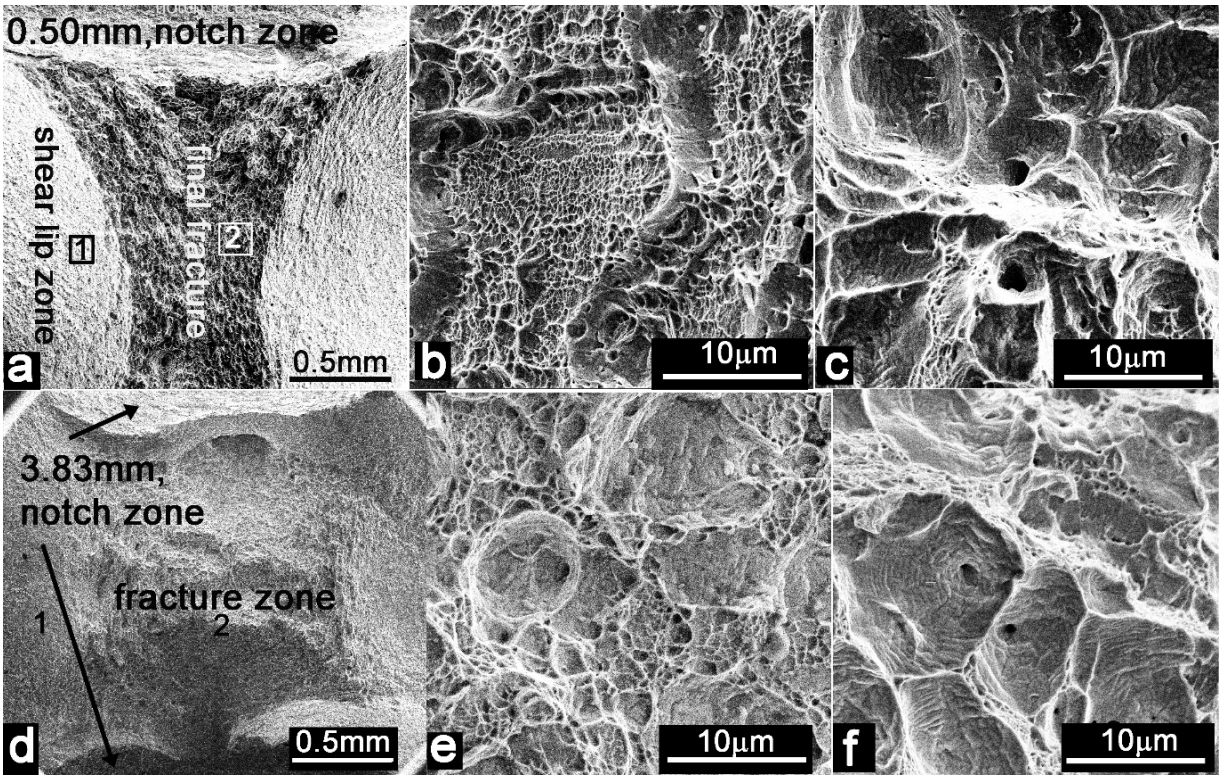

Fig. 11. SEM images of fracture surfaces in various Cu-Ag-Zr wire samples. In (a-c), the NTR is 0.50 mm. In (a), both the shear lip zone and the final fracture zone are within the notch region. In (b), the side view of the fracture surface in the "1" region of the shear lip zone (identified in a) shows small parabolic-shaped dimples that indicate ductile fracture resulting from shear loading. (c) Top view of the dimples and ridges in region "1". In (d-f), the NTR is 3.83 mm. (d) Large spherical dimples (in a network of cup- and cone-style ridges and dips) resulting from tensile loads in the fracture region. (e) Image showing no shear lip zone on the fracture surface. (f) Round dimples and ridges in the fracture zone, viewed from the top.

4. Conclusion

Uniaxial tension experiments, coupled with local strain measurements, were conducted to investigate the notch sensitivity of high-strength copper matrix composites, specifically Cu-alumina and Cu-Ag-Zr bulk wires. Notch-strengthening was observed in both composites for notch tip radii (NTRs) exceeding 0.20 mm. Localized yielding occurred within two strain-concentration bands originating from the notches, with their positions influenced by the notch tip radius. Smaller NTRs resulted in greater separation between the strain-concentration bands and the notch segments. In samples with small notches, these bands formed elliptical loops

connecting the notches, whereas larger notches shifted the bands toward the notch segment centers.

The response to notches differed markedly between nano-alumina-reinforced Cu-alumina and fiber-reinforced Cu-Ag-Zr composites. Cu-alumina exhibited no notch blunting under tensile deformation, while Cu-Ag-Zr showed significant blunting, indicating greater plastic deformation capacity. In unnotched samples, Cu-Ag-Zr wires demonstrated higher local plastic deformation in necked regions (up to 50%) compared to Cu-alumina (34%). In notched Cu-alumina, local elongation decreased rapidly with smaller NTRs, whereas in Cu-Ag-Zr, the decrease was notably slower.

These contrasting behaviors stem from microstructural differences. In Cu-alumina, pre-existing decohesion between alumina particles and the Cu matrix facilitated crack initiation, with notches accelerating crack propagation and connection, thus sharply reducing local elongation. In Cu-Ag-Zr, the realignment of Ag fibers mitigated the impact of notches, slowing the decline in local elongation. The notch insensitivity of Cu-Ag-Zr wires is attributed to their fiber-reinforced microstructure, which provides more malleable interfaces and greater flaw tolerance compared to the particle-reinforced Cu-alumina.

ACKNOWLEDGMENT

This work was undertaken in the National High Magnetic Field Laboratory, which is funded by US NSF (DMR-1644779). Furthermore, we would like to express our gratitude to Jens Freudenberger and Alexander Gaganov for discussion and supplying the Cu-Ag-Zr wire. We thank Mary Tyler for editing.

Data availability

The data supporting this study are available upon request.

References

[1] J.B. Dubois, L. Thilly, F. Lecouturier, P. Olier, P.O. Renault, Cu/Nb Nanocomposite Wires Processed by Severe Plastic Deformation for Applications in High Pulsed Magnets: Effects of the Multi-Scale Microstructure on the Mechanical Properties, IEEE Transactions on Applied Superconductivity 22(3) (2012) 6900104-6900104.

[2] L. Thilly, J. Colin, F. Lecouturier, J.P. Peyrade, J. Grilhé, S. Askénazy, Interface instability in the drawing process of copper/tantalum conductors, Acta Materialia 47(3) (1999) 853-857.

[3] J.D. Verhoeven, W.A. Spitzig, L.L. Jones, H.L. Downing, C.L. Trybus, E.D. Gibson, L.S. Chumbley, L.G. Fritzemeier, G.D. Schnittgrund, Development of deformation processed copper-refractory metal composite alloys, Journal of Materials Engineering 12(2) (1990) 127-139.
[4] K. Han, Strength and Ductility of Nanostructured Composites with Co-Deformable Components, Materials Science Forum 633-634 (2010) 383-392.
[5] R. Niu, K. Han, Strain hardening and softening in nanotwinned Cu, Scripta Materialia 68(12) (2013) 960-963.
[6] T.J. Miller, S.J. Zinkle, B.A. Chin, STRENGTH AND FATIGUE OF DISPERSION-STRENGTHENED COPPER, Journal of Nuclear Materials 179 (1991) 263-266.
[7] K. Han, R.E. Goddard, V. Toplosky, R. Niu, J. Lu, R. Walsh, Alumina Particle Reinforced Cu Matrix Conductors, Ieee Transactions on Applied Superconductivity 28(3) (2018) 1-5.
[8] B. An, Y. Xin, R. Niu, J. Lu, E. Wang, K. Han, Hardening Cu-Ag composite by doping with Sc, Materials Letters 252 (2019) 207-210.
[9] K. Han, J. Lu, V. Toplosky, R. Niu, R. Goddard, Y. Xin, R. Walsh, I. Dixon, V. Pantsyrny, Properties of Selected High-Strength Composite Conductors With Different Strengthening Components, IEEE Transactions on Applied Superconductivity 30(4) (2020) 1-5.
[10] A. Morozova, R. Mishnev, A. Belyakov, R. Kaibyshev, Microstructure and Properties of Fine Grained Cu-Cr-Zr Alloys after Termo-Mechanical Treatments, REVIEWS ON ADVANCED MATERIALS SCIENCE 54(1) (2018) 56-92.
[11] M. Jovanovj , V. Rajkovic, High electrical conductivity Cu-based alloys, Part I, Metalurgija 15 (2009) 125-133.
[12] S. Tardieu, D. Mesguich, A. Lonjon, F. Lecouturier-Dupouy, N. Ferreira, G. Chevallier, A. Proietti, C. Estournès, C. Laurent, Influence of alloying on the tensile strength and electrical resistivity of silver nanowire: copper composites macroscopic wires, Journal of Materials Science 56(7) (2021) 4884-4895.
[13] S. Tardieu, D. Mesguich, A. Lonjon, F. Lecouturier, N. Ferreira, G. Chevallier, A. Proietti, C. Estournès, C. Laurent, Nanostructured 1% silver-copper composite wires with a high tensile strength and a high electrical conductivity, Materials Science and Engineering: A 761 (2019) 138048.
[14] Y. Sakai, H.J. SchneiderMuntau, Ultra-high strength, high conductivity Cu-Ag alloy wires, Acta Materialia 45(3) (1997) 1017-1023.
[15] C. Zhao, R. Niu, Y. Xin, D. Brown, D. McGuire, E. Wang, K. Han, Improvement of properties in Cu–Ag composites by doping induced microstructural refinement, Materials Science and Engineering: A 799 (2021) 140091.
[16] C. Zhao, X. Zuo, E. Wang, R. Niu, K. Han, Simultaneously increasing strength and electrical conductivity in nanostructured Cu–Ag composite, Materials Science and Engineering: A 652 (2016) 296-304.
[17] N. Ageew, M. Hansen, G. Sachs, Segregation and property changes supersaturated silver-copper alloys, Zeitschrift Fur Physik 66(5-6) (1930) 350-376.
[18] Y.Z. Tian, S.D. Wu, Z.F. Zhang, R.B. Figueiredo, N. Gao, T.G. Langdon, Microstructural evolution and mechanical properties of a two-phase Cu–Ag alloy processed by high-pressure torsion to ultrahigh strains, Acta Materialia 59(7) (2011) 2783-2796.
[19] B. An, Y. Xin, R. Niu, Z. Xiang, Y. Su, J. Lu, E. Wang, K. Han, Stacking fault formation and Ag precipitation in Cu-Ag-Sc alloys, Materials Characterization 189 (2022) 111965.
[20] A. Gaganov, J. Freudenberger, E. Botcharova, L. Schultz, Effect of Zr additions on the microstructure, and the mechanical and electrical properties of Cu–7 wt.%Ag alloys, Materials Science and Engineering: A 437(2) (2006) 313-322.
[21] F. Bittner, S. Yin, A. Kauffmann, J. Freudenberger, H. Klauß, G. Korpala, R. Kawalla, W. Schillinger, L. Schultz, Dynamic recrystallisation and precipitation behaviour of high strength and highly conducting Cu–Ag–Zr-alloys, Materials Science and Engineering: A 597 (2014) 139-147.

[22] A. Gaganov, J. Freudenberger, W. Grünberger, L. Schultz, Microstructural evolution and its effect on the mechanical properties of Cu–Ag microcomposites, International Journal of Materials Research 95(6) (2004) 425-432.
[23] J.D. Verhoeven, H.L. Downing, L.S. Chumbley, E.D. Gibson, The resistivity and microstructure of heavily drawn Cu‐Nb alloys, Journal of Applied Physics 65(3) (1989) 1293-1301.
[24] W. Grunberger, M. Heilmaier, L. Schultz, Development of high-strength and high-conductivity conductor materials for pulsed high-field magnets at Dresden, Physica B 294 (2001) 643-647.
[25] W. Grunberger, M. Heilmaier, L. Schultz, Microstructure and mechanical properties of Cu-Ag microcomposites for conductor wires in pulsed high-field magnets, Zeitschrift Fur Metallkunde 93(1) (2002) 58-65.
[26] K. Han, A. Baca, H. Coe, J. Embury, K. Kihara, B. Lesch, L. Li, J. Schillig, J. Sims, S. Van Sciver, H.J. Schneider-Muntau, Material issues in the 100 T non-destructive magnet, Ieee Transactions on Applied Superconductivity 10(1) (2000) 1277-1280.
[27] Y. Leprince-Wang, K. Han, Y. Huang, K. Yu-Zhang, Microstructure in Cu–Nb microcomposites, Materials Science and Engineering: A 351(1) (2003) 214-223.
[28] L.-P. Deng, B.-S. Wang, H.-L. Xiang, X.-F. Yang, R.-M. Niu, K. Han, Effect of Annealing on the Microstructure and Properties of In-situ Cu–Nb Microcomposite Wires, Acta Metallurgica Sinica (English Letters) 29(7) (2016) 668-673.
[29] L. Deng, K. Han, K.T. Hartwig, T.M. Siegrist, L. Dong, Z. Sun, X. Yang, Q. Liu, Hardness, electrical resistivity, and modeling of in situ Cu–Nb microcomposites, Journal of Alloys and Compounds 602 (2014) 331-338.
[30] K. Yu-Zhang, J.D. Embury, K. Han, A. Misra, Transmission electron microscopy investigation of the atomic structure of interfaces in nanoscale Cu–Nb multilayers, Philosophical Magazine 88(17) (2008) 2559-2567.
[31] C. Krüger, A. Mortensen, In situ copper–alumina composites, Materials Science and Engineering: A 585 (2013) 396-407.
[32] X. Zhang, C. Lin, S. Cui, Z. Li, Characteristics of Nano-alumina Particles Dispersion Strengthened Copper Fabricated by Reaction Synthesis, Rare Metal Materials and Engineering 45(4) (2016) 893-896.
[33] Z. Xiao, Y. Huang, C. Chen, Z. Li, S. Gong, Y. Huang, C. Zhang, X. Zhang, Effects of thermal treatments on the residual stress and micro-yield strength of Al2O3 dispersion strengthened copper alloy, Journal of Alloys and Compounds 781 (2019) 490-495.
[34] R. Mishnev, I. Shakhova, A. Belyakov, R. Kaibyshev, Deformation microstructures, strengthening mechanisms, and electrical conductivity in a Cu–Cr–Zr alloy, Materials Science and Engineering: A 629 (2015) 29-40.
[35] R. Niu, V. Toplosky, K. Han, Cryogenic Temperature Properties and Secondary Phase Characterization of CuCrZr Composites, IEEE Transactions on Applied Superconductivity 32(6) (2022) 1-5.
[36] C. Salvan, L. Briottet, T. Baffie, L. Guetaz, C. Flament, CuCrZr alloy produced by laser powder bed fusion: Microstructure, nanoscale strengthening mechanisms, electrical and mechanical properties, Materials Science and Engineering: A 826 (2021) 141915.
[37] R. Niu, V.J. Toplosky, J.W. Levitan, J. Lu, K. Han, Deformation induced precipitation in CuCrZr composites, Materials Science and Engineering: A 875 (2023) 145092.
[38] X. Tang, X. Chen, F. Sun, L. Li, P. Liu, H. Zhou, S. Fu, A. Li, A study on the mechanical and electrical properties of high-strength CuCrZr alloy fabricated using laser powder bed fusion, Journal of Alloys and Compounds 924 (2022) 166627.
[39] J. Lu, T. Adkins, I. Dixon, D. Nguyen, K. Han, Nondestructive testing of high strength conductors for high field pulsed magnets, IEEE Transactions on Applied Superconductivity 30(4) (2020) 1-5.
[40] G.E. Dieter, Mechanical Behavior Under Tensile and Compressive Loads[1], Mechanical Testing and Evaluation, ASM International, 2000, p. 0.

[41] X.W. Gu, Z. Wu, Y.-W. Zhang, D.J. Srolovitz, J.R. Greer, Flaw-driven failure in nanostructures, arXiv preprint arXiv:1307.3182 (2013).
[42] T.A. Furnish, B.L. Boyce, J.A. Sharon, C.J. O'Brien, B.G. Clark, C.L. Arrington, J.R. Pillars, Fatigue stress concentration and notch sensitivity in nanocrystalline metals, Journal of Materials Research 31(6) (2016) 740-752.
[43] P. Lorenzino, A. Navarro, Grain size effects on notch sensitivity, International Journal of Fatigue 70 (2015) 205-215.
[44] H. Gao, B. Ji, I.L. Jager, E. Arzt, P. Fratzl, Materials become insensitive to flaws at nanoscale: lessons from nature, Proc Natl Acad Sci U S A 100(10) (2003) 5597-600.
[45] S. Kumar, X. Li, A. Haque, H. Gao, Is Stress Concentration Relevant for Nanocrystalline Metals?, Nano Letters 11(6) (2011) 2510-2516.
[46] J. Freudenberger, A. Kauffmann, H. Klauss, T. Marr, K. Nenkov, V.S. Sarma, L. Schultz, Studies on recrystallization of single-phase copper alloys by resistance measurements, Acta Materialia 58(7) (2010) 2324-2329.
[47] A. Gaganov, J. Freudenberger, E. Botcharova, L. Schultz, Effect of Zr additions on the microstructure, and the mechanical and electrical properties of Cu-7 wt.%Ag alloys, Materials Science and Engineering a-Structural Materials Properties Microstructure and Processing 437(2) (2006) 313-322.
[48] A. Gaganov, J. Freudenberger, W. Grunberger, L. Schultz, Microstructural evolution and its effect on the mechanical properties of Cu-Ag microcomposites, Zeitschrift Fur Metallkunde 95(6) (2004) 425-432.
[49] K. Han, J.D. Embury, J.R. Sims, L.J. Campbell, H.J. Schneider-Muntau, V.I. Pantsyrnyi, A. Shikov, A. Nikulin, A. Vorobieva, The fabrication, properties and microstructure of Cu–Ag and Cu–Nb composite conductors, Materials Science and Engineering: A 267(1) (1999) 99-114.
[50] R. Niu, K. Han, Pockets of strain-softening and strain-hardening in high-strength Cu-24wt%Ag sheets, Journal of Materials Science 58(21) (2023) 8981-8989.
[51] R.T. Qu, M. Calin, J. Eckert, Z.F. Zhang, Metallic glasses: Notch-insensitive materials, Scripta Materialia 66(10) (2012) 733-736.
[52] J. Rösler, M. Bäker, H. Harders, Plasticity and failure, in: J. Rösler, M. Bäker, H. Harders (Eds.), Mechanical Behaviour of Engineering Materials: Metals, Ceramics, Polymers, and Composites, Springer Berlin Heidelberg, Berlin, Heidelberg, 2007, pp. 63-118.
[53] R. Niu, K. Han, Effect of Notch Geometry on the Plastic Behavior of Cu-Ag Composites, IEEE Transactions on Applied Superconductivity 34(5) (2024) 1-5.
[54] R. Niu, K. Han, Z. Xiang, L. Qiao, T.M. Siegrist, Ultra-high local plasticity in high-strength nanocomposites, Journal of Materials Science 55(31) (2020) 15183-15198.